Nanotechnology **22** (2011) 275705 (6pp) doi:10.1088/0957-4484/22/27/275705

Achieving chiral resolution in self-assembled supramolecular structures through kinetic pathways

Jong Keon Yoon[1], Won-joon Son[2], Howon Kim[1], Kyung-Hoon Chung[1], Seungwu Han[2] and Se-Jong Kahng[1]

[1] Department of Physics, Korea University, 1-5 Anam-dong, Seongbuk-gu, 136-713, Seoul, Korea
[2] Department of Materials Science and Engineering, Seoul National University, Seoul 151-744, Korea

E-mail: sjkahng@korea.ac.kr

Received 27 March 2011
Published 20 May 2011
Online at stacks.iop.org/Nano/22/275705

Abstract

Chiral phase transitions were studied in a self-assembled 2,6-dibromoanthraquinones supramolecular system prepared on Au(111) using scanning tunneling microscopy. As the molecules were deposited at about 150 K, they formed heterochiral chevron structures (a racemate) consisting of two alternating prochiral molecular rows. When the as-deposited sample was warmed to 300 K followed by cooling to 80 K, phase-separated homochiral structures (a conglomerate), as well as the chevron structures, were observed. We propose molecular models for the structures that are in good agreement with *ab initio* studies and can be explained by hydrogen bonds and halogen bonds. We found that heterochiral chevron structures were more stable than homochiral structures due to two additional O $\cdots$ Br halogen bonds per molecule. We considered kinetic pathways for the phase transitions that were made possible via a disordered liquid phase entropically stabilized at 300 K. We show how chiral resolution can be achieved by exploiting kinetic paths allowed in supramolecular systems.

(Some figures in this article are in colour only in the electronic version)

1. Introduction

Achieving chiral resolution in molecular systems has been a longstanding and important problem due to its potential applications in heterogeneous catalysis, nonlinear optics, and drug screening [1, 2]. It is a difficult problem because nature prefers chiral intermixing over separation in the growth of molecular crystals. Also it is difficult to detect the chirality of individual molecules and molecular domains. On crystal surfaces, scanning tunneling microscopy (STM) has been used as a powerful tool to visualize various chiral structures of molecules such as pinwheel arrays [3–6], lamella layers [7–11], chiral clusters [12, 13], and directional chains [14–16]. Some of the structures are made of prochiral molecules whose chirality is obtained by symmetry breaking in adsorption geometries on surfaces, and a few molecular systems disclosed two-dimensional (2D) chiral phase transitions [17]. In the derivatives of naphthalene [18], benzoic acid [19], and quinacridone molecules [20], coverage-driven chiral phase transitions have been observed from a conglomerate (phase-separated homochiral) to a racemate (intermixed heterochiral) at low and high molecular coverages, respectively. This is caused by the competing balances between intermolecular bonds and molecule–substrate interactions under given packing constraints at different coverages. In prochiral guanine molecules on Au(111), a temperature-driven chiral phase transition was observed in hydrogen bonded 2D networks [21]. A conglomerate grew in the room temperature deposition of molecules, and transformed to a racemate by annealing to 400 K with subsequent cooling to 150 K. This was explained by considering the entropy contribution from the dynamic fluctuations of two different racemic structures at high temperature. The direction of the phase transitions

 © 2011 IOP Publishing Ltd Printed in the UK & the USA

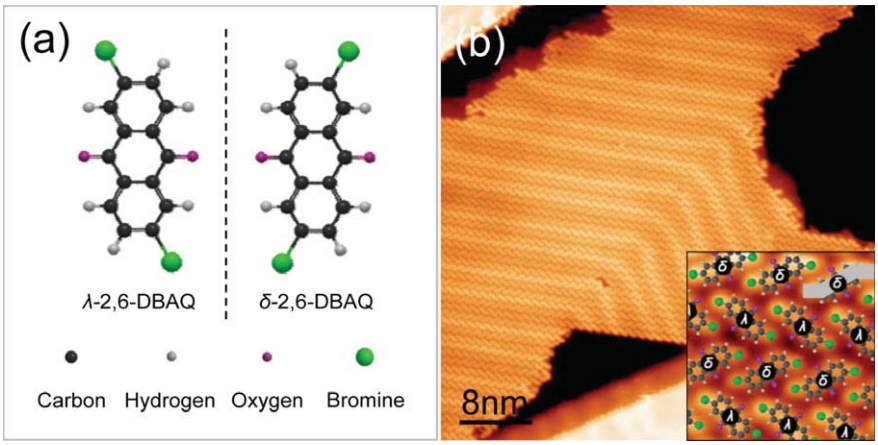

Figure 1. (a) Chemical structures of a 2,6-dibromoanthraquinone (DBAQ) molecule. The prochiral species encountered upon adsorption are labeled λ and δ. (b) Typical STM images, measured at 80 K, of the 2D supramolecular structures of 2,6-DBAQ molecules as-deposited at about 150 K. Alternating λ- and δ-DBAQ molecular rows are denoted in the inset of (b). Sizes of STM images: (b) 48×48 nm^2 and tunneling current: $I_T = 0.1$ nA. Sample voltage: $V_S = -1.8$ V.

in these examples was to loose chiral resolution, from a conglomerate to a racemate. However, a practical problem in chiral chemistry is how to achieve chiral resolution from a racemate to a conglomerate, which has not yet been studied in two dimensions.

In this paper, we report on the observations of a temperature-driven prochiral phase transition occurring from a racemate to a conglomerate in self-assembled 2,6-dibromoanthraquinones (DBAQ) molecules on Au(111) using STM. When the as-deposited racemate sample was warmed to 300 K followed by cooling to 80 K, some of conglomerate structures were found, as well as racemate structures. The molecular model and energy gain of the racemate structure were previously studied by our group [22]. The molecular model for the newly observed conglomerate structures is proposed in the present paper. It was well reproduced by *ab initio* studies and compared with previous racemate results. We found that the racemate was more stable than the conglomerate due to two additional O$\cdots$Br halogen bonds. The chiral phase transitions toward a less stable conglomerate structure were mediated by the third phase—a disordered liquid, entropically stabilized at high temperature. The phase transition took place partially such that there were both racemate and conglomerate structures afterward.

2. Experimental section

All STM experiments were performed using a home-built STM housed in an ultra-high vacuum chamber with a base pressure below 7×10^{-11} Torr. The Au(111) surface was prepared from a thin film (200 nm thick) of Au on mica that was exposed to several cycles of Ar-ion sputtering and annealing at 800 K over the course of 1 h. The surface cleanliness of the Au(111) was checked by observing typical herringbone structures on the terraces in the STM images. Commercially available 2,6-DBAQ (Tokyo Chemical Industry) was outgassed in a vacuum for several hours and then deposited on the Au(111) at submonolayer coverage by thermal evaporation using an alumina-coated evaporator. STM images were obtained at constant-current mode with a Pt/Rh tip while keeping the sample temperature at 80 K. A conglomerate (parallel arrays) was observed by warming up a racemate (chevrons) sample to 300 K for 4 h, then, the sample was returned to a cold stage at 80 K. The estimated average warming and cooling rate was $\sim$5 K min^{-1}.

3. Theoretical calculations

We performed *ab initio* density-functional calculations using the VASP code [23, 24]. The interaction between ions and electrons was approximated by the projector-augmented wave (PAW) potential [25]. The generalized gradient approximation (GGA) with the Perdew–Burke–Ernzerhof (PBE) functional was used to describe the exchange correlations between electrons [26]. The energy cutoff for the plane wave basis was set to 600 eV. To describe non-bonding interactions between the molecules, particularly the van der Waals type, an empirical correction scheme proposed by Grimme *et al* was adopted [27]. The energy and electrostatic potential for the isolated molecules were obtained using a $35 \times 35 \times 20$ Å^3 supercell. A simulation cell containing two DBAQ molecules was adopted to describe the periodic structure. The height of the simulation box perpendicular to the molecule plane was fixed at 10 Å, and the lateral cell parameters were optimized such that the residual stress was reduced to under 1 kbar.

4. Results and discussion

DBAQ molecules are achiral in the gas and liquid phases. However, they are prochiral on 2D surfaces because it is hard to flip over an adsorbed molecule. Figure 1(a) shows two different prochiral molecules named λ-DBAQ and δ-DBAQ. Typical STM images of DBAQ structures deposited at about 150 K are shown in figure 1(b), and a model is superimposed over the image in the inset of figure 1(b) [22].

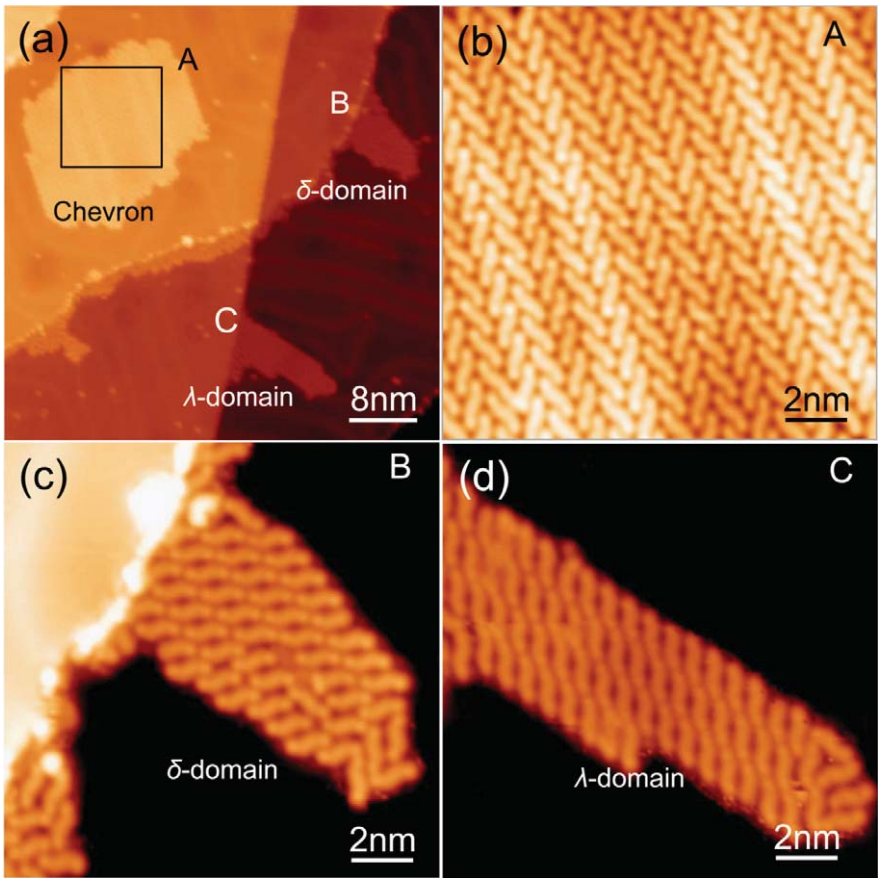

Figure 2. (a) A large area STM image obtained after warming to 300 K and subsequent cooling to 80 K, containing intermixed chevrons and phase-separated homochiral λ and δ domains. (b) Reappeared chevron structures enlarged from the square in (a). Enlarged STM images of (c) δ and (d) λ domains from (a). Sizes of STM images: (a) 51 × 51 nm^2. (b)–(d) 14 × 14 nm^2. Tunneling current: $I_T = 0.1$ nA. Sample voltage: $V_S = -1.8$ V.

Individual molecules showed crank-like shapes, and the self-assembled structures showed chevron structures consisting of two alternating molecular rows. The prochiral direction of each molecule in chevron structures is denoted as either λ or δ in the inset of figure 1(b). It is clear that prochiral directions were preserved within a row, but alternated from row to row. This means that the chevron structures are an intermixed prochiral racemate of the DBAQ molecules. The molecular structure and intermolecular bonds were previously studied [22].

New structures were observed when the as-deposited DBAQ racemate was warmed to 300 K and then cooled to 80 K. Figure 2 shows a large area and the enlarged STM images obtained after such processes. Chevrons reappeared in figure 2(b). New parallel array structures appeared, and are shown in figures 2(c) and (d). The molecular island in figure 2(c) is made of δ-DBAQ only, making a homochiral δ-domain of DBAQ, whereas the island in figure 2(d) is composed of λ-DBAQ molecules, forming a homochiral λ-domain. The intermolecular arrangements of these δ and λ domains are mirror-symmetric to each other. They constitute a phase-separated conglomerate of prochiral DBAQ molecules. These phases grew both at the step edges and terraces of the surface. In most cases, δ and λ domains were observed simultaneously, observed in an STM image of 100 nm × 100 nm, implying local population conservation.

A molecular model for parallel array structures is overlaid on an STM image in figure 3(b), enlarged from (a). Here only the structure of the δ-domain will be discussed, because the structure of the λ-domain can be obtained by symmetry consideration. Figure 3(c) shows five molecules extracted from the model with the simplified version of electrostatic potential distributions, and also shows intermolecular bonds related to the center DBAQ molecule [22]. Along a row (the direction of the arrow in figure 3(c)), the center molecule had eight intermolecular bonds (four O···H and four Br···H bonds), as depicted by black dotted lines. Across a row, the center molecule had four Br···H intermolecular bonds, as depicted with red dotted lines. Thus, these parallel arrays had six intermolecular bonds per molecule: two O···H and three Br···H bonds.

To understand the precise arrangement of DBAQ molecules in parallel arrays, we performed *ab initio* calculations based on density-functional theory. The calculation results, shown in figure 3(d), clearly reproduced our models. Two unit cell vectors formed a parallelogram with a 77.1° angle. The equilibrium lattice distances were 0.80 nm and 1.25 nm, which are consistent with experimental observations (76.3° ± 0.5°, 0.77 ± 0.05 nm, and 1.28 ± 0.05 nm). Since the characteristic features of our models are

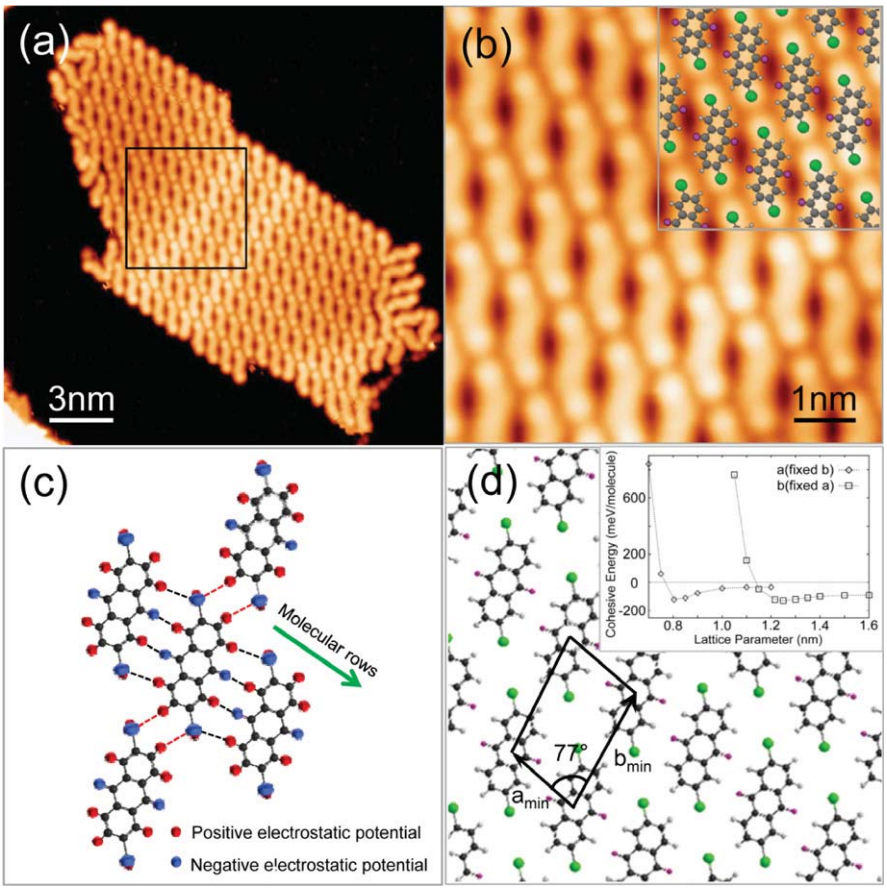

Figure 3. (a) An STM image of a λ-homochiral domain. (b) The molecular model is superimposed over the STM image enlarged from a square in (a). (c) Schematic illustrations for five 2,6-DBAQ molecules extracted from (b) with simplified electrostatic potential distributions around H, O, and Br atoms. The dotted lines indicate possible intermolecular bonds. (d) Calculated results of the relaxed homochiral structure of 2,6-DBAQ molecules from *ab initio* study based on density-functional theory. Two unit cell vectors form a parallelogram unit cell. The energy gain per molecule is drawn in the inset of (d) as a function of lattice parameters. Only the results along two lines for fixed $a = 0.80$ nm and fixed $b = 1.25$ nm are displayed for simplicity. Squares are the results of the calculations, and the curves represent fittings. The sizes of the STM images are (a) 20×20 nm^2 and (b) 7×7 nm^2. Tunneling current: $I_T = 0.1$ nA. Sample voltage: $V_S = -1.8$ V.

Table 1. Bond distances from calculation and sum of the van der Waals radii as reference.

	Bond distance (nm)		
Intermolecular bond	Chevrons (racemate)	Parallel arrays (conglomerate)	Sum of the van der Waals radii (nm)
O···H	0.28	0.23	0.28
O···Br	0.35	—	0.34
Br···H	0.29, 0.28	0.34, 0.32	0.30

in good agreement with the calculation results, quantitative bond distances were extracted from the calculation results as summarized in table 1. As references, the distances were compared with the sum of the van der Waals radii of two bonded atoms [22, 28]. Since a typical width of intermolecular potential is 0.1 nm, the bond distances of three different kinds of intermolecular bonds in DBAQ structures were quite close to the reported sum of the van der Waals radii. This confirms that these three bonds are real entities of our molecular structures. Two neighboring Br atoms have a head-to-head configuration. They will repulse each other because there are positive electrostatic potentials at the end of both heads. However, the distance between the two Br atoms was 0.50 nm, which is too large compared to the sum of the van der Waals radii, to significantly affect to the stability of molecular structures.

The energy gains of the molecular structures can be roughly estimated by considering the bond strengths and the number of each intermolecular bond. In previous bulk experiments and calculations, the strengths (distances) of O···H, Br···H, and O···Br bonds under similar molecular environments (covalently bonded to C atoms) were about 50 meV (0.28 nm), 70 meV (0.30 nm), and 60 meV (0.38 nm), respectively [29–32]. Chevrons have two O···H, four Br···H, and two O···Br bonds per molecule, and parallel arrays have two O···H and four Br···H bonds per molecule [22]. Therefore, the expected energy gains for chevrons and parallel arrays are 500 meV and 380 meV per molecule, respectively. In table 2, we summarize the energy gains obtained from the *ab initio* calculations for chevrons and parallel arrays. We used two different methods for the calculations: a generalized gradient approximation (GGA) and

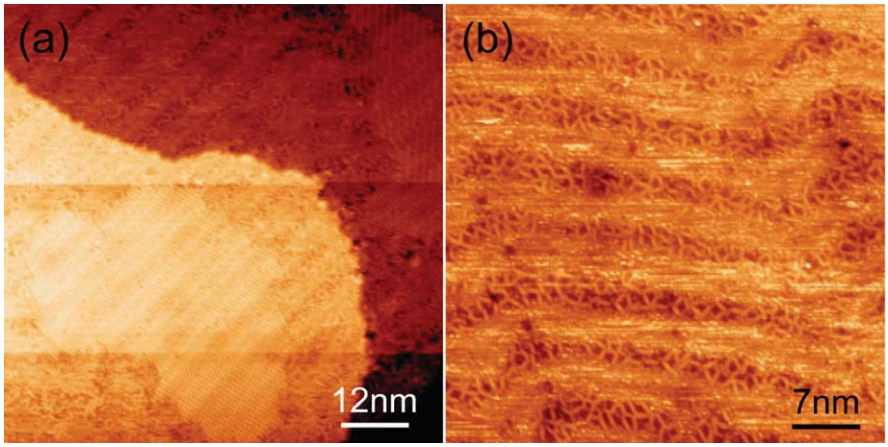

Figure 4. (a) and (b) STM images of disordered areas frozen directly from a liquid phase before forming ordered chevrons or simple arrays. The sizes of the STM images are (a) 78 × 78 nm^2 and (b) 45 × 45 nm^2. Tunneling current: $I_T = 0.1$ nA. Sample voltage: $V_S = -2.0$ V.

Table 2. Energy gains per molecule from two different calculation methods.

	Chevrons (racemate)	Parallel arrays (conglomerate)
GGA/PBE	−184	−122
GGA + van der Waals corrections	−472	−352

a GGA with van der Waals corrections (GGA + wdW). GGA with van der Waals corrections showed energy gains closer to the aforementioned rough estimation. Since energy gains reflect every detail of molecular bond configurations such as bond distances and angles, calculation results may not exactly reproduce estimation. Chevrons have larger energy gains than parallel arrays by 60–130 meV per molecule (6–12 kJ mol^{-1}). Therefore, chevrons (a racemate) are more stable than parallel arrays (a conglomerate) in a self-assembled DBAQ system. The origin of this energy difference can be found in the two additional O···Br halogen bonds of chevrons. These additional bonds are also related to the different overall aspect ratio of the chevrons and parallel arrays. As shown in figure 2, the aspect ratio of molecular islands in chevrons along and across molecular rows is close to one. This implies that the sticking probabilities along and across rows in chevrons are comparable to each other, which is explained by a model that has equal numbers (with similar strengths) of intermolecular bonds across and along a row. On the other hand, the aspect ratio in parallel arrays is larger than two. This means that the sticking probability along a row is larger than the sticking probability across a row in parallel arrays, which is also explained by a model that has twice as many intermolecular bonds across a row than along a row.

We considered possible kinetic pathways of the phase transitions from chevrons to parallel arrays. When DBAQ molecules were deposited at 150 K, they diffused on Au(111) to form chevrons that were energetically favored over parallel arrays. As an as-deposited sample warmed up, molecules were dissociated from the edges of chevron islands. It has been reported that such edge dissociation can occur at about 300 K, including molecular systems that have stronger intermolecular bonds (about 1 eV per molecule) than DBAQ bonds, and that well-ordered molecular structures coexist with a disordered 2D liquid phase of molecules [33–35]. Likewise, DBAQ molecules may have a 2D liquid phase at 300 K that coexists with chevron structures. The liquid phase can be stabilized by an entropy contribution. As the sample is cooled to 80 K, the liquid phase can either transform to chevrons or parallel arrays. Still, we observed that about twice as many molecules formed chevrons as formed parallel arrays. Cooling processes allowed the system to have both structures due to kinetic limitations. In some regions, we were able to observe the molecular islands of parallel arrays surrounded by disordered molecules, as shown in figure 4(a). The molecules in these regions were frozen directly from a liquid phase before they formed ordered chevrons or parallel arrays. The shapes of molecules were only resolved at the face-centered cubic (fcc) regions of Au(111) herringbone structures in the disordered structures shown in figure 4(b). Other regions remained fuzzy, possibly due to mobile or vibrating molecules at 80 K [33].

5. Conclusion

In conclusion, we studied the chiral phase transitions of DBAQ on Au(111) using STM. The as-deposited molecules formed heterochiral chevron structures, and some of them transformed to phase-separated homochiral parallel array structures by warming to 300 K followed by cooling. Molecular models for the structures were proposed and were well reproduced by *ab initio* studies. The models can be explained using the calculated electrostatic potential distributions. Chevrons were more stable than parallel arrays due to two additional O···Br halogen bonds per molecule. We considered kinetic paths for the phase transitions that were made possible via a disordered liquid phase entropically stabilized at 300 K. Our study showed that exploiting kinetic paths can be a way to achieve chiral resolution in 2D molecular systems, which should be applicable to other chiral molecular systems.

Acknowledgments

The authors gratefully acknowledge financial support from the National Research Foundation of Korea, and from the Ministry of Education Science and Technology of the Korean government (grant nos 2005-2002369, 2007-0054038, 2010-0018781 and 2010-0025301). WS and SH were supported by the Quantum Metamaterials Research Center (grant no. R11-2008-053-03001-0).

References

[1] Amabilino D B (ed) 2009 *Chirality at the Nanoscale: Nanoparticles, Surfaces, Materials and More* (Weinheim: Wiley–VCH)
[2] Ernst K-H 2006 *Top. Curr. Chem.* **265** 209
[3] Fasel R, Parschau M and Ernst K-H 2003 *Angew. Chem. Int. Edn* **42** 5178
[4] Miura A, Jonkheijm P, De Feyter S, Schenning A P H J, Meijer E W and De Schryner F C 2005 *Small* **1** 131
[5] Blüm M-C, Cávar E, Pivetta M, Patthey F and Schneider W-D 2005 *Angew. Chem. Int. Edn* **44** 5334
[6] Katsonis N *et al* 2008 *Angew. Chem. Int. Edn* **47** 4997
[7] De Feyter S, Grim P C M, Rücker M, Vanoppen P, Meiners C, Sieffert M, Valiyaveettil S, Müllen K and De Schryver F C 1998 *Angew. Chem. Int. Edn* **37** 1223
[8] Qiu X, Wang C, Zeng Q, Xu B, Yin S, Wang H, Xu S and Bai C 2000 *J. Am. Chem. Soc.* **122** 5550
[9] Tao F and Bernasek S L 2005 *J. Phys. Chem.* B **109** 6233
[10] Rohde D, Yan C-J, Yan H-J and Wan L-J 2006 *Angew. Chem. Int. Edn* **45** 3996
[11] Chen Q, Chen T, Wang D, Liu H-B, Li Y-L and Wan L-J 2010 *Proc. Natl Acad. Sci. USA* **107** 2769
[12] Böhringer M, Morgenstern K, Schneider W-D and Berndt R 1999 *Angew. Chem. Int. Edn* **38** 821
[13] Böhringer M, Morgenstern K, Schneider W-D and Berndt R 1999 *Phys. Rev. Lett.* **83** 324
[14] Weckesser J, De Vita A, Barth J V, Cai J V C and Kern K 2001 *Phys. Rev. Lett.* **8709** 096101
[15] Chen Q and Richardson N V 2003 *Nat. Mater.* **2** 324
[16] Kim B-I, Cai C, Deng X and Perry S S 2003 *Surf. Sci.* **538** 45
[17] Raval R 2009 *Chem. Soc. Rev.* **38** 707
[18] Böhringer M, Schneider W-D and Berndt R 2000 *Angew. Chem. Int. Edn* **39** 792
[19] Vidal F, Delvigne E, Stepanow S, Lin N, Barth J V and Kern K 2005 *J. Am. Chem. Soc.* **127** 10101
[20] Yang B, Wang Y, Cun H, Du S, Xu M, Wang Y, Ernst K-H and Gao H-J 2010 *J. Am. Chem. Soc.* **132** 10440
[21] Xu W, Kelly R E A, Gersen H, Lægsgaard E, Stensgaard I, Kantorovich L N and Besenbacher F 2009 *Small* **5** 1952
[22] Yoon J K, Son W-J, Chung K-H, Kim H, Han S and Kahng S-J 2011 *J. Phys. Chem.* C **115** 2297
[23] Kresse G and Hafner J 1993 *Phys. Rev.* B **47** 558
[24] Kresse G and Hafner J 1994 *Phys. Rev.* B **49** 14251
[25] Blöchl P E 1994 *Phys. Rev.* B **50** 17953
[26] Perdew J P, Burke K and Ernzerhof M 1996 *Phys. Rev. Lett.* **77** 3865
[27] Grimme S 2004 *J. Comput. Chem.* **25** 1463
[28] Rowland R S and Taylor R 1996 *J. Phys. Chem.* **100** 7384
[29] Pawin G, Solanki U, Kwon K-Y, Wong K L, Lin X, Jiao T and Bartels L 2007 *J. Am. Chem. Soc.* **129** 12056
[30] Futami Y, Kudoh S, Ito F, Nakanaga T and Nakata M 2004 *J. Mol. Struct.* **690** 9
[31] Riley K E, Murray J S, Politzer P, Concha M C and Hobza P J 2009 *J. Chem. Theory Comput.* **5** 155
[32] Auffinger P, Hays F A, Westhof E and Ho P S 2004 *Proc. Natl Acad. Sci. USA* **101** 16789
[33] Barth J V, Weckesser J, Trimarchi G, Vladimirova M, De Vita A, Cai C, Brune H, Günter P and Kern K 2002 *J. Am. Chem. Soc.* **124** 7991
[34] Marschall M *et al* 2010 *ChemPhysChem* **11** 1446
[35] Merz L, Parschau M, Zoppi L, Baldridge K K, Siegel J S and Ernst K-H 2009 *Angew. Chem. Int. Edn* **48** 1966